Intense magnetic fields in the atmosphere of the Sun

S S Hasan
Indian Institute of Astrophysics, Koramangala, Bangalore-560034, India
email : hasan@iiap.res.in

1. Introduction

Magnetic fields are believed to play a key role in the dynamics and activity on the Sun and other late-type stars, involving a complex interaction between the field and plasma. This activity occurs at all levels in the solar atmosphere. In the photosphere it gives rise to sunspots, whose distribution with time exhibits a 11-year cycle for reasons which are still not fully understood. Bright areas called *faculae* near spots and the overlying *plages* associated with enhanced chromospheric heating are another manifestation of magnetic activity. In the corona, prominences or filaments which are cool and dense structures, can become active and erupt. Another example of magnetic activity are solar flares, which represent a sudden (on a time scale of about 1 hour) release of large energy (10^{29}–10^{32} erg) in the form of radiation and fast particles. Coronal mass ejections (CMEs), which represent the ejection of coronal matter into space, are yet another example of activity.

As already stated, the magnetic field is responsible for the above forms of activity. However, the above-mentioned phenomena are not entirely distinct, but in fact represent a response of the solar plasma to changes in the underlying magnetic field topology and dynamics. Active regions on the Sun are believed to form due to the emergence of bipolar magnetic flux from the convection zone. This field is responsible for the rich diversity of processes in the solar atmosphere. Magnetic flux upon emerging in the photosphere, gets concentrated into discrete structures which range from sunspots at the largest scale down to tiny *faculae*. Any progress in understanding the different forms of activity must necessarily focus on the physics of magnetic flux tubes at different locations, ranging from the deep convection zone to the upper atmosphere.

In this review, we shall focus on the nature of magnetic elements associated with strong magnetic fields (outside of sunspots) that extend through the surface layers of the Sun. In Section 2, we discuss the properties of photospheric magnetic structures as well as mechanisms that can intensify the field to the observed strengths (typically in the kilogauss range). Section 3 deals with dynamical processes associated with magnetic flux tubes and their role in heating the chromosphere and corona. Finally in Section 4 we present a summary and the broad conclusions of our review.

2. Nature of surface magnetic fields

It is well known that the magnetic field on the surface of the Sun primarily consists of discrete elements, varying in size from 50 000 km in the largest sunspots down to 100–300 km in intense flux tubes, with field strengths in the range 1500–2000 G (e.g., [1]; see also the review [2], and references therein). More extended structures such as *plages* and the chromospheric network consist of assemblies of intense flux tubes. *Plages* are the chromospheric manifestations of *faculae*, photospheric field elements that appear as bright structures. The network essentially consists of a pattern that defines the boundaries of large cells called supergranules. Magnetic flux tubes typically fill about 30% of the total surface area in a *plage*. In this study we focus on the small-scale magnetic field

and exclude sunspots, mainly because limitations of space prevent us from doing adequate justice to this topic. The reader is referred to several excellent monographs on this subject [3,4].

It is generally believed that the magnetic field on the Sun as well as in many stars is generated through a dynamo action, which according to current understanding occurs in a shear layer just below the base of the convection zone, where strong toroidal fields can be stably stored for sufficiently long for field amplification to occur. Magnetic flux is injected into the photosphere from the interior in the form of bipolar concentrations. They emerge as coherent flux tubes in the photosphere on a wide range of scales. The source function $n(A)$ of the frequency of emerging bipolar regions as a function of area A is a smooth monotonically decreasing function of A [5]. How does the distribution of flux-tube size continue to flux tubes with smaller diameters below the resolution limit? Although it is not possible to determine the number of individual flux tubes in a *plage*, one can attempt a qualitative estimate. Let us compare the area in active region *plages* (including the region between flux tubes) with that occupied by sunspots. The ratio of the *plage* to sunspot area changes from 12 at cycle maximum to 25 at minimum [6], which implies that the surface area of *plages* is much larger than than of sunspots. Taking into account the magnetic elements in the network of the quiet Sun, increases the ratio even further. Since 10–20% of the surface area is typically covered by fields in a *plage*, the amount of magnetic flux carried by *plages* and sunspots is comparable at maximum [7].

Upon emergence as large coherent entities (the largest one being sunspots), flux tubes fragment into the enhanced network. Active regions survive in this *plage* state for several days depending upon their size [8,9]. Harvey [8] finds a typical time given approximately by $15(\Phi/10^{21}\,\mathrm{Mx})$ days, where Φ is the total magnetic flux. Once active regions begin their decay, the flux escapes from them into the quiet photosphere, where it is passively moved by the supergranule flows to the boundaries and into the network, where it cancels and replaces the old flux. The emerging flux is at about the dynamic equipartition field strength B_{eq}. For a typical flow speed $v \approx 2\,\mathrm{km\ s^{-1}}$, the dynamic equipartition field $B_{\mathrm{eq}} \approx 400$ G. Consequently, some local process must be present which not only resists the tendency of the field elements to fragment, but also intensifies the magnetic field to the observed values in the kG range.

2.1. Formation of intense flux tubes in the photosphere

It is is generally believed that the formation of intense flux tubes occurs through a combination of two mechanisms: viz. *flux expulsion* [10] and *convective collapse* [11].

2.1.1. Flux expulsion

Flux expulsion is the interaction of convection with a vertical magnetic field, leading to the expulsion of the field from the interior of a convection cell to its boundaries, which can be quantitatively studied using the well known induction equation given by:

$$\frac{\partial \mathbf{B}}{\partial t} = \nabla \times (\mathbf{v} \times \mathbf{B}) + \eta \nabla^2 \mathbf{B}\,, \tag{1}$$

where $\mathbf{B}$, $\mathbf{v}$ and η denote the magnetic field, velocity and magnetic diffusivity respectively. The latter is related to the electrical conductivity σ by the relation $\eta = c^2/4\pi\sigma$, where c is the speed of light. Since the electrical conductivity of the solar plasma is very high, one should in principal be able to generate very high field strengths. This process has been extensively studied numerically [12-16].

These calculations show that the convective flows concentrate the magnetic field in filament

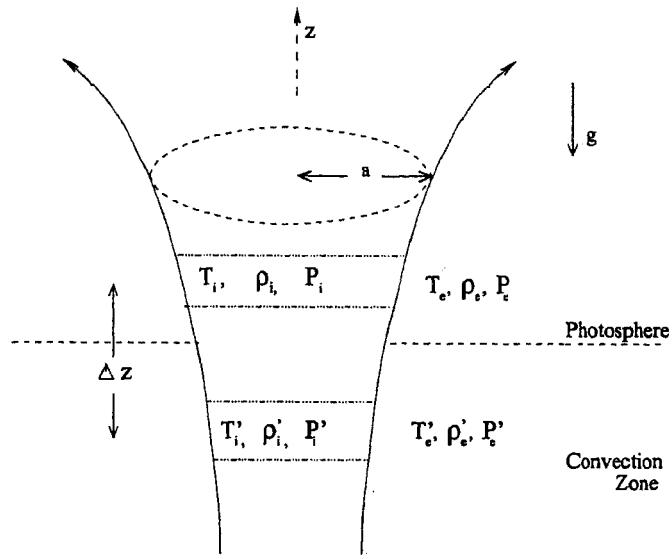

Figure 1: Physical explanation for the occurrence of a convective instability in a vertical magnetic flux tube extending vertically through the photosphere and convection zone. The atmosphere inside and outside the tube is initially in hydrostatic equilibrium and the internal and external temperatures are equal at each geometric level. Consider a small downward adiabatic displacement Δz of a fluid element. Assuming that this element remains in pressure equilibrium with the ambient medium, it will experience a negative buoyancy if the temperature gradient inside the tube is greater than the adiabatic value. For more details see the discussion in the text.

channels located in regions between the edges of the convective cells, which are also the sites of cool downflowing material.

However, when one includes the back-reaction of the field on the flow, it appears unlikely that the maximum field strengths that can be achieved by this process can exceed the dynamical equipartition value of several hundred Gauss. This suggests that some other mechanism is needed to intensify the field further to strengths observed in the magnetic network. A possible way of achieving this is through *convective collapse.*

2.1.2. Convective collapse:

Convective collapse is an instability driven by the super-adiabatic temperature gradient just below the photosphere, which was first suggested by Parker [11] as a mechanism responsible for the formation of intense flux tubes on the Sun. In order to understand this process, let us consider a "thin" vertical flux tube of cylindrical cross-section on the solar surface extending through the photosphere and into the convection zone of the Sun. By "thin" we mean that all physical quantities in the tube at a particular height (z) are essentially constant in the radial direction. Let us idealize the tube as a tapered cylinder (see Fig. 1) whose cross-section increases with height (in view of the decrease of confining external pressure) and focus on a gas element in the tube at a height z with temperature T_i, density ρ_i and pressure p_i. Initially we assume that the tube is in hydrostatic equilibrium, so

that the vertical force F_z acting on this element is:

$$F_z = -g\rho_i - \frac{dp_i}{dz} = 0\,, \tag{2}$$

where g is the acceleration due to gravity (acting in the downward direction).

Equation (2) expresses a balance between the buoyancy and pressure forces. We now displace this gas element downward by a distance $\Delta z < 0$. At the new location z', let the temperature, density and pressure be denoted by T_i', ρ_i' and p_i' respectively. The force acting on the fluid element at the displaced position is given by:

$$F_z' = -g\rho_i' - \frac{dp_i'}{dz} \tag{3}$$

Writing $F_z' = F_z + \Delta F_z$ along with similar expressions for ρ_i' and p_i', where ΔF_z, the Lagrangian perturbation in the force F_z on the fluid element, is given by:

$$\Delta F_z = -g\Delta\rho_i - \frac{d\Delta p_i}{dz}\,. \tag{4}$$

For an adiabatic displacement,

$$\frac{\Delta\rho_i}{\rho_i} = \frac{1}{\gamma\chi_\rho}\frac{\Delta p_i}{p_i}, \tag{5}$$

where γ is the ratio of specific heats and χ_ρ is defined by (12).

Let us assume that that the gas inside the tube is achieves instant pressure balance with its surroundings so that:

$$p_i + \frac{B^2}{8\pi} = p_e\,, \tag{6}$$

where p_e is the external pressure.

If the internal and external temperatures are equal so that $T_i = T_e$ (thermal equilibrium), then since $p_i < p_e$, the gas in the tube is less dense than its surroundings ($\rho_i < \rho_e$), implying that the tube will rise under the influence of gravity.

Using Eq.(6), we find:

$$\Delta p_i = \frac{\beta}{\beta+1}\Delta p_e = \frac{\beta}{\beta+1}\frac{dp_e}{dz}\Delta z \tag{7}$$

where $\beta = 8\pi p_i/B^2$. Substituting (5) and (7) in (4), we find:

$$\begin{aligned}\Delta F_z &= -\frac{\beta}{\beta+1}\rho_e g\left(\frac{1}{\gamma\chi_\rho}\frac{d\ln p_e}{dz} + \frac{1}{\rho_e g}\frac{d^2p_e}{dz^2}\right)\Delta z \\ &= -\frac{\beta}{\beta+1}\rho_e\omega_{\rm BV}^2\Delta z\,,\end{aligned} \tag{8}$$

assuming that the external gas is in hydrostatic equilibrium at all heights.

In Eq.(8), $\omega_{\rm BV}^2$ denotes the Brunt-Väisälä frequency given by:

$$\omega_{\rm BV}^2 = -g\left[\frac{d\ln\rho}{dz} - \frac{1}{\gamma\chi_\rho}\frac{d\ln p}{dz}\right], \tag{9}$$

$$= -g\frac{\chi_T}{\chi_\rho}\left(\left|\frac{d\ln T}{dz}\right| - \left|\frac{d\ln T}{dz}\right|_{\rm ad}\right), \tag{10}$$

$$= -\gamma\frac{g^2}{c_S^2}\,\chi_T\,(\nabla - \nabla_{\rm ad}), \tag{11}$$

where $\nabla \equiv d\ln T/d\ln p$, $c_S = \sqrt{\gamma\chi_\rho\, p/\rho}$ is the sound speed and for convenience we have dropped the subscript 'e' on all quantities appearing in the right hand side of the expression for $\omega_{\rm BV}^2$. The quantities χ_ρ and χ_T (which incorporate the effects of ionization) are defined by:

$$\chi_\rho = \left(\frac{\partial \ln p}{\partial \ln \rho}\right)_T$$
$$\chi_T = \left(\frac{\partial \ln p}{\partial \ln T}\right)_\rho \tag{12}$$

The second term inside the brackets in Eq.(10) denotes the temperature gradient if the stratification were adiabatic. Thus, $\omega_{\rm BV}^2$ is a measure of the super-adiabaticity of the fluid. If $\omega_{\rm BV}^2 < 0$, we find from Eq.(8), that the displaced fluid element experiences a downward force, which implies that the configuration is unstable. Thus, the condition for instability is:

$$\left|\frac{d\ln T}{dz}\right| > \left|\frac{d\ln T}{dz}\right|_{\rm ad}, \tag{13}$$

or alternatively if $\nabla > \nabla_{\rm ad}$. which is the well-known Schwarzschild criterion for convective instability.

We see that as the field strength increases (i.e., as β decreases) the force on the displaced element decreases, which implies that the magnetic field has an inhibiting effect on the instability.

Physically, the above instability occurs because a gas element (for a super-adiabatic stratification) that is displaced downward finds itself in an environment where it is cooler and denser than its immediate surroundings and therefore experiences a negative buoyancy. The instability has the effect of evacuating the upper portion of the tube (just below the photosphere which is super-adiabatic), leading to a local reduction in pressure. Consequently, the tube collapses to a configuration with a higher field strength to maintain pressure balance with the ambient medium. The enhanced field resists the tendency of the tube to collapse. A careful analysis based on a linear stability calculation, reveals that *convective collapse* occurs if $\beta > \beta$ where β_c denotes the value for marginal stability [17-19], For the solar stratification, Spruit & Zweibel [18] found $\beta_c = 1.83$, which corresponds to a surface value of the magnetic field strength of about 1300 G, whereas Rajaguru & Hasan [20] obtained $\beta_c = 1.64$ using a slightly different solar model.

Detailed nonlinear calculations have been carried out for *thin* flux tubes [21-27] and for a 2-D flux sheet [28] in order to follow the time dependent evolution of the instability. For closed boundary conditions at both ends of the tube (consistent with the linear results of Spruit & Zweibel [18]), Hasan [22] found that a tube with surface field of about 700 G (corresponding to $\beta \approx 3$) undergoes collapse to a state in which the field has an average strength of about 1250 G. For an adiabatic flow, the fluid in the tube is unable to get rid of its momentum and in the final state it exhibits oscillations. On the other hand, it was argued by Takeuchi [26] that if one adopts an open boundary condition at the bottom, the fluid in the tube eventually settles down to hydrostatic equilibrium. It should be noted that field intensification occurs mainly in the surface layers, i.e., locally in a layer ~ 100 km below the photospheric surface. Calculations [22,23] suggest that the field does not increase much above the marginal stability limit of $\beta \approx 1.8$, whereas observations suggest a lower value ($\beta \approx 0.3$) (e.g., [2] and references therein). In the author's opinion, no convincing calculation has yet demonstrated how such strong fields can be generated. A possible clue to this problem might lie in the fact that intense flux tubes occur in regions associated with cool downflowing plumes of gas. Preliminary calculations were carried out by Hasan & Ballegooijen [29] in which the inclusion of Reynolds stresses and the cool material just outside the tube were incorporated in an equilibrium model for a flux tube. These authors found that Reynolds stresses are likely to play an important

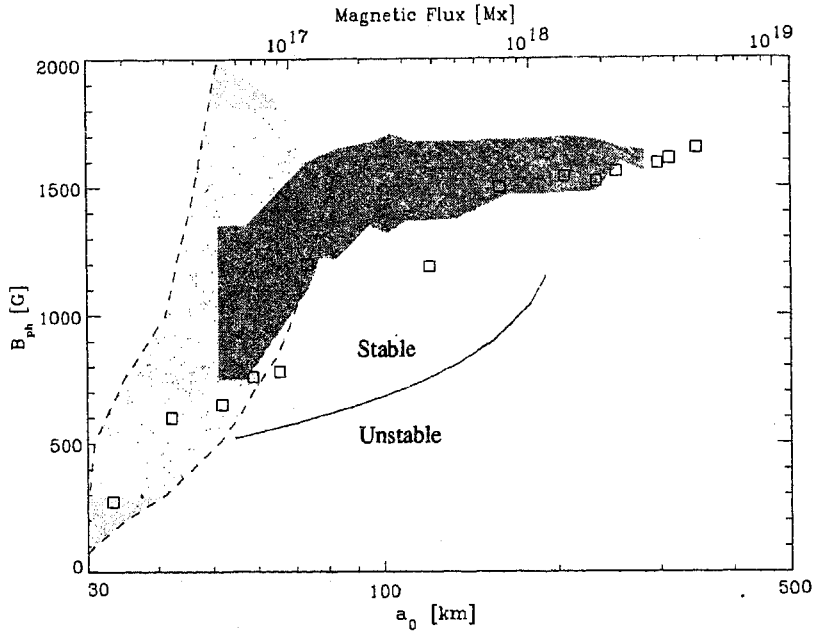

Figure 2: Relationship between the critical photospheric radius a_0 and photospheric field strength $B_{\rm ph}$ (solid line) which demarcates the separation between convectively stable and unstable tubes. The top scale denotes the magnetic flux. Superposed are data from observations: squares are from Solanki et al. [31]; the light shaded region from Lin [32] and Lin & Rimmele [33]; and the dark shaded region is from Sánchez Almeida & Lites [34]. All points above the *solid* curve denote stable configurations whereas those below are unstable. A flux tube that is unstable will trace out a vertical path (since magnetic flux is conserved for an ideal plasma) in this diagram

role in producing intense fields with high field strength.

2.2 Energy transport in flux tubes

The analysis presented in the preceding section assumed an adiabatic energy equation i.e., external energy sources or sinks were absent. Let us now consider the consequences of including lateral heat exchange between the flux tube and the external medium. It can be shown [30] that the effect of horizontal radiative transport is to counteract the instability, which is most efficient when the gas within the tube is thermally insulated from its surroundings. However, in reality this insulation is reduced due to the leakage of heat into the tube from the ambient medium. Since the time scale for radiative heat exchange decreases with tube radius, the critical value of β for the onset of instability (β_c) increases with decreasing photospheric radius [30]. The situation becomes more complicated if one also incorporates vertical radiative transport, which has a destabilizing effect and tends to enhance the convective collapse due to a cooling associated with radiative losses in the vertical direction ([20]). Using a refined treatment of radiative transfer Rajaguru & Hasan [20] derived a relation between the critical photospheric radius a_0 and the photospheric field strength $B_{\rm ph}$, which demarcates the separation between convectively unstable and stable tubes. Figure 2 depicts the

variation (solid curve) of $B_{\rm ph}$ as a function of the photospheric radius $a_{\rm ph}$ (the magnetic flux $B\pi a_{\rm ph}^2$ is shown on the upper scale). For comparison, we also show data from observations: the squares are from Solanki et al. [31]; the light shaded region from Lin [32] and Lin & Rimmele [33]; and the dark shaded region is from Sánchez Almeida & Lites [34]. All points above the solid curve denote stable configurations whereas those below are unstable. A flux tube that is unstable (region below the solid curve) will trace out a vertical path (since magnetic flux is conserved for an ideal plasma) in this diagram. Once it crosses the solid curve, the collapse will cease and the tube will be stable. We find that the maximum field strength for which the tube is unstable is 1160 G, corresponding to $\beta_c = 2.45$ and a critical radius of $a_0 = 190$ km, which translates to a critical flux $\Phi_c = 1.31 \times 10^{18}$ Mx. Tubes with a magnetic flux greater than Φ_c are invariably in a collapsed state with a field above 1160 G. Figure 2 suggests a division of observed tubes into two groups with: (a) flux concentrations with flux above Φ_c which are associated with kilogauss strong-field network elements in which their field strength is weakly dependent on their flux content [31]; and (b) elements with flux lower than Φ_c in which the field has a significant variation with flux. Such flux tubes can be identified with weak to moderate fields, which may possibly occur in the internetwork region, that is the interior of the supergranulation cells.

The above discussion has focused on the relation between the critical field strength and radius for stability. Let us now consider the situation for $\beta < \beta_c$. In this case, it can be shown that the tube exhibits overstability [20,23,30]. Physically, overstability involves a delicate balance among the following three processes: (a) buoyancy, which drives the convective instability in the presence of a superadiabatic temperature gradient, (b) a restoring force associated with the magnetic and gas pressure, and (c) a dissipative mechanism such as radiative damping. When the magnetic field is strong enough to counteract the instability, the tube exhibits undamped oscillations in the adiabatic limit. However, in the presence of lateral radiative transport, which depends on the flux tube radius, the driving force due to buoyancy is reduced in such a way that the net restoring force is greater during the return to equilibrium than it is during the departure away from equilibrium. Consequently, during each oscillation cycle, energy is extracted from the radiation field and converted into mechanical motions. However, for field strengths that are typical in the solar network ($\beta \approx 0.3$), the time scale for damping in the vertical direction becomes sufficiently small so as to counteract the overstability which is driven by lateral heat exchange. Rajaguru & Hasan [20] found that such flux tubes with radius greater than about 170 km are no longer overstable but undergo radiative damping.

Having discussed the methods by which intense magnetic fields are generated in the surface layers and some of their properties, let us now turn out attention to dynamical phenomena occurring in flux tubes.

3. Dynamics of magnetic flux tubes

3.1. Background

In the solar atmosphere (photosphere and chromosphere) one needs to distinguish the magnetic network on the boundary of supergranulation cells, where strong magnetic fields are organized in magnetic flux tubes, and internetwork regions in the cell interior, where magnetic fields are weak and dynamically unimportant. In the middle chromosphere (i.e., at a height of about 1000 km above the photosphere), the filling factors of the network and internetwork regions are typically in the ratio of 2 to 3.

The network is about 30% brighter in Ca II K_{2v} emission than the internetwork chromosphere medium [35]. Both the network and the internetwork medium show *bright points* (BPs), which are

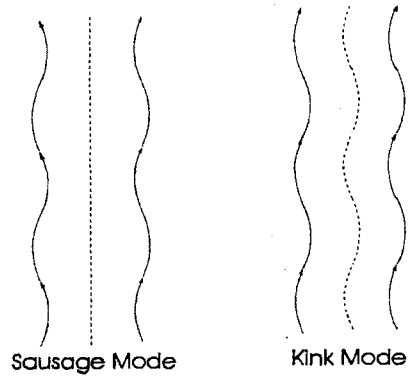

Figure 3: Form of the perturbation associated with sausage (left panel) and kink (right panel) waves in a magnetic flux tube

prominent in the emission peaks in the cores of the Ca II H and K lines, formed in the middle chromosphere. However, the dynamical and spectral properties of network and internetwork BPs are quite different. In internetwork areas the chromospheric velocity power spectrum is dominated by oscillations with frequencies at and above the acoustic cutoff frequency (period 3 min in the upper photosphere), whereas in the network Ca II H line center velocity and intensity power spectra are dominated by low-frequency oscillations with periods of 5-20 min [36]. These long-period waves have also been observed at larger heights [37-39]. Furthermore, network BPs show high emission in the line core for a significant fraction of their lifetime [36], whereas internetwork BPs have a bright phase that lasts only about 5% of the wave period. Finally, 80% of network BPs have symmetric profiles in the line core, with more or less equal intensity in the blue and red emission peaks on either side of the central absorption. In contrast, only about 30% of internetwork BPs have symmetric profiles, and 40% have blue-peak enhancements [40], hence the name H_{2v} or K_{2v} bright points.

While the qualitative properties of internetwork BPs are reasonably well understood, including their formation in regions with upward-propagating acoustic shocks that encounter downward-flowing gas [41], this is not true for network BPs. The physical processes that heat the magnetic network have not been identified. Are network BPs heated by wave dissipation, and if so, what is the nature of these waves? How can we understand the observed relatively constant emission and symmetric line profiles of network BPs? The source of energy for network BPs is likely to be magneto-hydrodynamic waves. However, an identification of the the wave modes responsible for these oscillations and the mechanism by which they are excited are still not fully understood. In this section, we shall focus on dynamical processes occurring in the network and their role in heating the magnetic chromosphere. We shall also present some new results on waves in the magnetic network.

3.2. Longitudinal and transverse waves in flux tubes

The magnetic field in the network can be idealized in terms of isolated vertical flux tubes in the photosphere which fan out with height. It is well known that flux tubes support a variety of wave modes. The detailed behaviour of these modes for thin flux tubes has been extensively studied (for a recent review see [42]). The modes that we shall be concerned with are the sausage or longitudinal mode [43,44] and the kink waves or transverse mode [45-47]. Figure 3 schematically shows the general form of the perturbations of the flux tube in the above modes.

The earliest studies on MHD wave excitation were based on extensions of the Lighthill mechanism [48-52]. More recently, the generation of longitudinal and transverse waves in a flux tube was examined through turbulent motions in the convection zone [53-56]. An alternative scenario motivated by observations [57,58] suggests that transverse waves can be generated through the impulse imparted by granules to magnetic flux tubes [59-61]. These investigations suggested that there is sufficient energy flux in MHD waves to account for chromospheric heating.

Let us consider in some detail consequences of MHD wave excitation in magnetic flux tubes through the buffeting action of convective motions (granulation) in the surrounding medium. Such waves are likely to play an important role in heating the magnetic chromosphere and also possibly the corona.

3.3. Linear model

Consider a vertical magnetic flux tube extending through the photosphere, which is assumed to be "thin" and isothermal. It is convenient to use the "reduced" displacement, $Q(z,t)$, which is related to the physical Lagrangian displacement, $\xi(z,t)$, by $Q(z,t) = \xi_\perp(z,t)e^{-z/4H}$, where H denotes the scale height of the atmosphere.

It can be shown that Q_α ($\alpha = \kappa$ for transverse waves and $\alpha = \lambda$ for longitudinal waves) satisfies a Klein–Gordon equation (Hasan & Kalkofen [62], henceforth HK).

$$\frac{\partial^2 Q_\alpha}{\partial z^2} - \frac{1}{c_\alpha^2}\frac{\partial^2 Q_\alpha}{\partial t^2} - k_\alpha^2 Q_\alpha = F_\alpha \,, \tag{14}$$

where $k_\alpha = \omega_\alpha / c_\alpha$, ω_α is the cutoff frequency for the wave and c_α is the wave propagation speed in the medium and F_α is a forcing function that parameterizes the impact delivered to the flux tube by a granule (for further details see HK).

The speeds for the transverse and longitudinal waves are respectively,

$$c_\kappa^2 = \frac{2}{\gamma}\frac{c_s^2}{1+2\beta} \,, \tag{15}$$

$$c_\lambda^2 = \frac{c_s^2}{1+\gamma\beta/2} \,, \tag{16}$$

where c_s is the sound speed, γ is the ratio of specific heats ($\gamma = 5/3$), $\beta = 8\pi p/B^2$, p is the gas pressure inside the tube and B is the magnitude of the vertical component of the magnetic field on the tube axis.

The cutoff frequencies for transverse and longitudinal waves are, respectively,

$$\omega_\kappa^2 = \frac{g}{8H}\frac{1}{1+2\beta} \,, \tag{17}$$

$$\omega_\lambda^2 = \omega_{BV}^2 + \frac{c_\lambda^2}{H^2}\left(\frac{3}{4} - \frac{1}{\gamma}\right)^2 \,, \tag{18}$$

where $\omega_{BV}^2 = g^2\,(\gamma - 1)/c_s^2$ is the Brunt-Väisälä frequency (which follows from [9] or [11]) for a fully ionized isothermal plasma.

Equation (14) can readily be solved using Green's functions (for details see HK). The generic behaviour for the impulsive excitation of transverse and longitudinal waves by granular motions in the magnetic network is the same: the buffeting action due to a single impact excites a pulse that propagates along the flux tube with the kink or longitudinal wave speed. For strong magnetic fields,

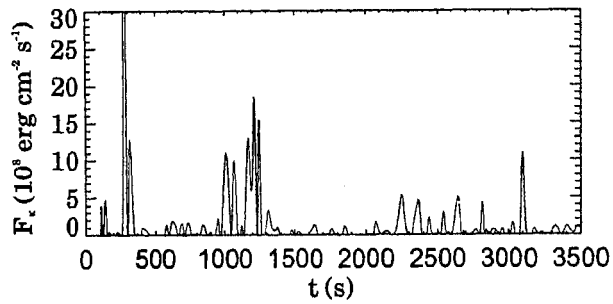

Figure 4: Time variation of the vertical energy flux in transverse waves in a single flux tube at $z = 750$ km due to footpoint motions taken from observations excited in an isothermal flux tube with $T = 6650$ K and $\beta = 0.3$.

most of the energy goes into transverse waves, and only a much smaller fraction into longitudinal waves, a result also found by Ulmschneider & Musielak [56]. After the passage of the pulse, the atmosphere gradually relaxes to a state in which it oscillates at the cutoff period of the mode. These results show that the first pulse carries most of the energy and after this pulse has passed the atmosphere oscillates in phase without energy transport. The period observed in the magnetic network is interpreted as the cutoff period of transverse waves, which leads naturally to an oscillation at this period (typically in the 7-minute range) as proposed by Kalkofen [63].

For weaker magnetic fields the energy fluxes in the two modes are comparable. From the absence of a strong peak at low frequencies in the power spectrum of the cell interior (CI) we conclude that both transverse and longitudinal waves must make a negligible contribution to K_{2v} bright point oscillations. The absence of the magnetic modes then implies that the waves in the CI are probably acoustic waves, and the observed 3 minute period is therefore the acoustic cutoff period – and not the cutoff period of longitudinal waves. This implies that the magnetic field structure in the CI is likely to be different from that of flux tubes in the magnetic network.

3.4. Chromospheric heating

The above discussion has considered the buffeting of flux tubes as a single impact. In reality, we expect the excitation of waves in a tube to occur not as a single impact but continually due to the highly turbulent and stochastic motion of granules. It is interesting to examine the consequences of this interaction for chromospheric heating. Such an investigation was carried out by Hasan, Kalkofen & van Ballegooijen ([64], hereafter HKB), who modelled the excitation of waves in the magnetic network due to the observed motions of G-band bright points, which were taken as a proxy for footpoint motions of flux tubes. Using high resolution observations of G band bright points in the magnetic network, the energy flux in transverse waves was calculated in a large number of magnetic elements.

Figure 4 shows the vertical energy flux in transverse waves versus time at a height $z = 750$ km for a typical magnetic element in the network. One finds that the injection of energy into the chromosphere takes place in brief and intermittent bursts, lasting typically 30 s, separated by longer periods (longer than the time scale for radiative losses in the chromosphere) with lower energy flux. Similar pulse-like time dependence, shown in Fig. 7, has also been found by Ulmschneider [65] and Ulmschneider & Musielak [56]. The peak energy flux into the chromosphere is as high as 10^9 erg

$cm^{-2}\ s^{-1}$ in a single flux tube although the time-averaged flux is $\sim 10^8$ erg $cm^{-2}\ s^{-1}$. However, from an observational point of view, such a scenario for heating the magnetic network, would yield a high variability with time in CaII emission, which appears incompatible with observations. A possible remedy to this difficulty would be to postulate the existence of other high-frequency motions (periods 5–50 s) which cannot be detected as proper motions of G-band bright points (HKB). Adding such high-frequency motions to the simulations of HKB yields much better agreement with the persistent emission observed from the magnetic network. For a filling factor of 10% at $z = 750$ km, the predicted flux $\sim 10^7$ erg $cm^{-2}\ s^{-1}$. This value is sufficient to balance the observed radiative loss of the chromospheric network (see Model F′ of Avrett [66]). Therefore, for transverse waves to provide a viable mechanism for *sustained* chromospheric heating, the main contribution to the heating must come from high-frequency motions, with typical periods 5–50 s. HKB speculated that the high-frequency motions could be due to turbulence in intergranular lanes, but some aspects of this model require further investigation.

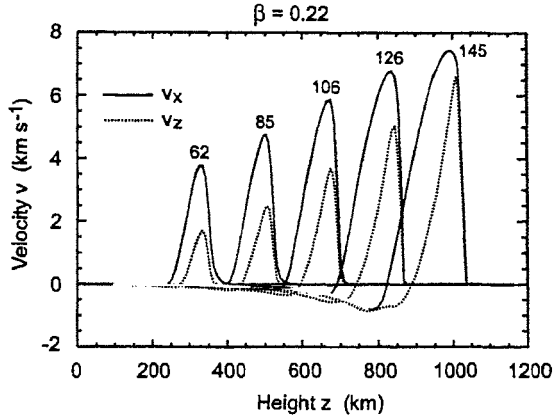

Figure 5: Nonlinear coupling of transverse and longitudinal waves in a flux tube: transverse velocity v_x (solid lines) and longitudinal v_z (dashed lines) as functions of height z at various times for $\beta = 0.22$, $t_0 = 20$ and $v_0 = 2.5$ km s^{-1} (after Hasan [70]). The numbers beside the curves denote the time in seconds.

3.4. Nonlinear results

The above studies modeled wave excitation and propagation in terms of the Klein-Gordon equation, motivated by the identification of the power peak near 7 min in the observed power spectrum [36-38] with the cutoff period of kink waves in thin magnetic flux tubes [63]. This analysis was based on a linear approximation in which the longitudinal and transverse waves are decoupled. However, it is well known that the velocity amplitude $v(z)$ for the two modes increases with height z (for an isothermal atmosphere $v \propto \exp[z/4H]$, where H is the pressure scale height), so that the motions are expected to become supersonic higher up in the atmosphere. At such heights, nonlinear effects become important, leading to a coupling between the transverse and longitudinal modes. Some progress on this question has been made in one dimension (1-D), using the nonlinear equations for a thin flux tube, by Ulmschneider et al. [67], Huang et al. [55], Zhugzhda et al. [68] and more recently by Hasan et al. [69] and Hasan & Ulmschneider [70], who examined mode coupling between transverse and longitudinal modes in the magnetic network.

3.4.1. 1-D Calculations

Let us consider a vertical "thin" flux tube initially in hydrostatic equilibrium and isothermal with a temperature $T = 6000$ K which is the same as that in the external medium, with a radius of 50 km and a field strength of $B = 1425$ G at $z = 0$, that corresponds to a plasma $\beta = 0.22$ (which by assumption remains constant with height. The radius of the tube increases with z as $\exp(z/4H)$.

The basic equations for adiabatic longitudinal-transverse MHD waves in a thin flux tube consist of a set of coupled differential equations [67], which are solved numerically using the method of characteristics. In the present work we adopt this method, modified to include shocks, based on the treatment of Zhugzhda et al. [68]. The computational domain in the vertical direction has an equidistant grid of size 9 km. The Courant condition is used to select the time step to advance the equations in time.

At the lower boundary, taken at $z = 0$, we assume that the flux tube has a transverse motion which consists of a single impulse with a velocity of the form:

$$v_x(0,t) = v_0 e^{-[(t-t_0)/\tau]^2} \tag{19}$$

where v_0 is the specified velocity amplitude, t_0 denotes the time when the motions have maximum amplitude and τ is the time constant of the impulse. The longitudinal component of the velocity at the base is assumed to be zero. In the present calculations we take $t_0 = 20$ s and $\tau = 5$ s.

At the upper boundary of the computational domain (at $z = 1200$ km) we use transmitting boundary conditions following Ulmschneider et al. [71], and assume that the velocity amplitude remains constant along the outward-propagating characteristics. The characteristic equations are used to self-consistently determine physical quantities at the boundary.

The initial equilibrium model is perturbed with a transverse motion at $z = 0$ in the form of an impulse with a velocity given by Eq.(19). This impulse generates a transverse wave that propagates upward with the kink wave tube speed c_κ, which is about 7.9 km s^{-1} for the equilibrium model. The resulting motion in the tube as a function of height and time follows from the time-dependent MHD equations for a thin flux tube.

Figure 5 shows the variation of the transverse v_x (solid lines) and longitudinal v_z (dashed lines) components of the velocity as a function of height z at various epochs of time t for $v_0 = 2.5$ km s^{-1}. The numbers beside the curves denote the time t (in s). We find that in the low part of the atmosphere, where the transverse velocity amplitude is small (compared to the kink wave speed c_κ), the longitudinal component of the velocity is negligibly small. As the initial pulse propagates upward, the transverse velocity amplitude increases. Due to nonlinear effects, which set in for a Mach number $M = v_x/c_\kappa$ as low as 0.2, longitudinal motions are generated. The efficiency of the nonlinear coupling increases with the amplitude of the transverse motions. When $v_x \approx c_\kappa$, the amplitudes in the transverse and longitudinal components become comparable. The longitudinal motions, being compressive, steepen with height and eventually form shocks. A shock is first formed at a height of 600 km. The compression associated with the longitudinal shock produces heating in the atmosphere.

Let us summarize the main conclusions to emerge from the above treatment. When the transverse velocities are significantly less than the kink wave speed (the linear regime), there is essentially no excitation of longitudinal waves. When the velocity amplitude of the pulse reaches about 20% of the kink wave speed, the kink wave pulse generates an acoustic-wave pulse, which is followed by a wake at the cutoff period of acoustic waves [69]. This behavior is different from the continuous excitation of a wave with a sinusoidally moving piston at a fixed frequency, for which the kink wave would generate an acoustic wave at twice the frequency of the kink wave, provided the frequency

of the acoustic wave would be higher than the acoustic-cutoff period (e.g. Ulmschneider [72]). The efficiency of mode coupling was found to depend on the magnetic field strength in the network and is a maximum for field strengths corresponding to $\beta \approx 0.2$, when the kink and tube wave speeds are almost identical. This can have interesting observational implications. Furthermore, even when the two speeds are different, once shock formation occurs, the longitudinal and transverse shocks exhibit strong mode coupling.

The energy transfer to longitudinal waves in the low-amplitude limit is proportional to the square of the kink wave velocity amplitude, indicating a nonlinear process; the effect saturates when the Mach number approaches unity, where the coupling becomes linear. In the low-amplitude limit, the generation of longitudinal modes from transverse modes is not reciprocated by the inverse process. The reason for this asymmetrical behavior is that gas particles in the transverse motion of kink waves have a longitudinal component, but the gas motion in longitudinal waves has no transverse component. In the high-amplitude limit the wave motion no longer separates into the two modes [68].

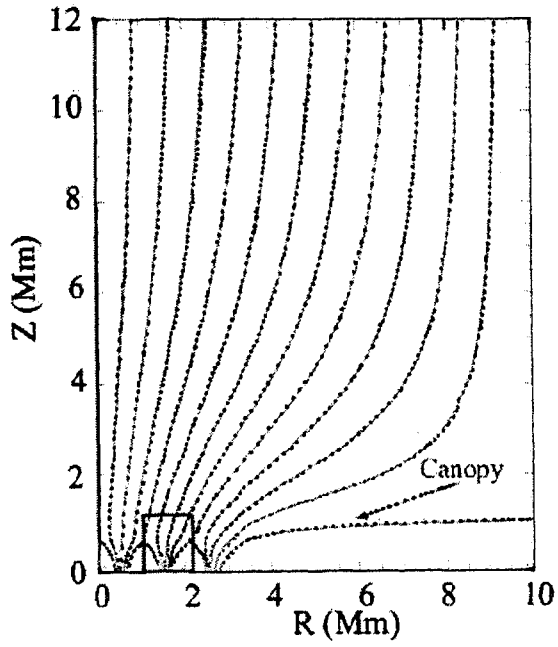

Figure 6: Model of a network element consisting of individual flux tubes separated at the photospheric surface by a distance of 1000 km which merge at a height of about 600 km. The small box in the lower left corresponds to the domain taken up for simulations (after Cranmer & Ballegoiijen [75]).

3.4.2. 2-D Calculations

The above studies on the magnetic network make use of two important idealizations: they assume that the magnetic flux tubes are thin, an approximation that becomes invalid at about the height of formation of the emission peaks in the cores of the H and K lines (typically at heights 1000-1500 km

above the photosphere); and they neglect the interaction of neighboring flux tubes. Some progress in this direction has recently been made by Rosenthal et al. [73] and Bogdan et al. [74] who studied wave propagation in a 2-D stratified atmosphere, assuming a potential magnetic field, to model the network and internetwork regions on the Sun. They examined the propagation of waves that are excited from a spatially localized source in the photosphere. Their results indicate that there is strong mode coupling between fast and slow MHD waves at the so-called magnetic canopy, which they identified with regions where the magnetic and gas pressures are comparable. As a consequence of the potential-field approximation, some magnetic field lines are nearly horizontal even at the base of the field. Such a model may not be appropriate for a network patch, which is perhaps better idealized as a collection of vertical tubes [75].

An alternative model can be developed based on the idea that flux tubes are anchored in subsurface layers where convective flows may be different from those in the visible photosphere. Flux tubes are located in convective downflows below intergranular lanes. These downflows are expected to be highly turbulent, involving lateral motions that produce transverse waves on the flux tubes. When the upward propagating waves reach the photosphere, they cause horizontal motions of flux tubes relative to their local surroundings. This generates excess pressure on the leading edge of a flux tube, and a pressure deficit on the trailing edge. Two dimensional MHD calculations that will be presented later in this section, indicate that these pressure pulses produce an upward-velocity pulse on the leading side of the flux tube and a downward pulse on the trailing side. These pressure pulses and vertical flows are an integral part of the MHD wave, so the transverse and longitudinal motions are strongly coupled.

Following Cranmer and van Ballegooijen [75], let us assume that a network element (with a typical flux $\sim 3 \times 10^{19}$ Mx) consists of a collection of smaller flux tubes that are spatially separated from each other in the photosphere. The gas pressure in the atmosphere decreases with increasing height, causing a lateral expansion of the flux tubes. Neighboring flux tubes within the network element merge into a monolithic structure at some height. Above this "merging height" the network element consists of a single thick flux tube that further expands with height. The outer edge of this tube forms a magnetic canopy that overlies the neighboring supergranular cells. A second merging occurs when neighboring network elements come together at a canopy height. Figure 6 schematically shows the picture we have for the network field structure. It consists of three distinct regions:

1. Photospheric region up to about 0.6 Mm, consisting of individual flux tubes, with a typical diameter of 100 km in the low photosphere. The flux tubes are rooted in intergranular lanes and are separated from one another by about the diameter of a granule ($\sim$ 1 Mm). They expand upward and merge with their neighbors at a height of about 0.6 Mm.

2. Lower chromosphere, between the heights of 0.6 and 1 Mm, the merged network flux element expands laterally over the surrounding supergranular cell-center and overlying field-free chromosphere;

3. Upper chromosphere and corona, between 1 and 12 Mm, the fully merged magnetic field fills the available volume. At larger heights, the field expands primarily in the vertical direction and becomes more or less uniform. However, at lower heights between 1 and 2 Mm, the field strength varies significantly with horizontal position, and the field strength directly above the flux tubes (left side of Figure 6) is much larger than that above the supergranular cell center (right side of Figure 6).

Let us consider wave generation in a single flux sheet in magnetostatic equilibrium. The computational domain consists of a square with a size of 1200 km. A uniform grid of 240 $\times$ 240 cells is used, corresponding to a grid spacing of 5 km. The width of the sheet at $z = 0$ is approximately 100

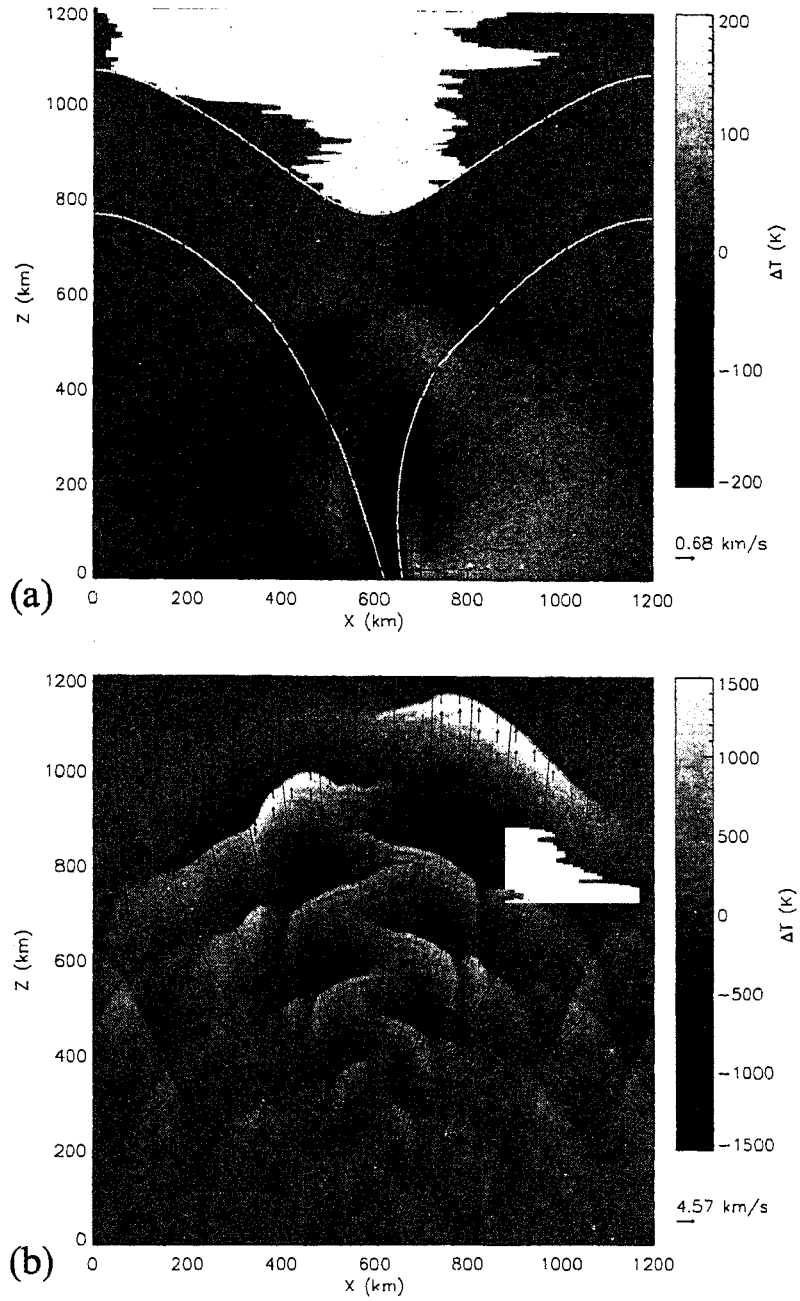

Figure 7: Results from two different simulations (after Hasan et al. [76]) at: (a) $t = 82$ s, corresponding to impulsive excitation; (b) $t = 136$ s, for periodic excitation with a period $P = 24$ s. In both cases the peak velocity is 0.75 km s^{-1}. The thin black curves are the magnetic field lines, the arrows are plasma velocity, the grey scale shows the temperature perturbations about the initial state and the white curves denote contours of constant β.

km, and the central field strength is 1530 G. Waves were excited by means of a transverse motion at the lower boundary ($z = 0$), which displaces the flux sheet. We used the following form for the transverse velocity:

$$v_x(x, 0, t) = v_0 \sin(2\pi t/P), \tag{20}$$

where v_0 is the specified velocity amplitude and P denotes the wave period. Figure 7 (taken from Hasan et al. [76]) shows results from two different simulations. In the first case (Fig. 7a), the flux sheet is displaced to the right for half a wave period ($P = 240$ s) and then stops. The peak velocity $v_0 = 750$ m s^{-1}, and the vertical velocity at the base is assumed to be zero. We refer to this case as impulsive excitation. Note the temperature excess and upward flow on the right side of the flux sheet, and the temperature deficit and downflow on the left side. These are due to the pressure fluctuations created by the right-ward displacement of the flux sheet, which generates a vortex motion with uplow and downflow motions on the right and left sides respectively. The top of the vortex motion is in the opposite direction to that at the base. As time proceeds, the vortex grows in size and also moves upward.

In the second case (Fig. 7b), a periodic motion with $P = 24$ s is applied indefinitely. The horizontal motion of the tube at the lower boundary is a source of acoustic waves in the ambient medium just outside the tube. These propagate freely upward into the unmagnetized medium as well as penetrating the flux tube where they get converted into slow modes propagating along field lines. Note that a series of shock waves develops in the chromosphere.

In summary, the above calculations demonstrate that horizontal displacements of a sheet cause compressions and decompressions of gas at its sides. This results in the generation of longitudinal waves that propagate up into the main body of the flux sheet as well as into the surrounding medium. At larger heights, longitudinal waves steepen into shocks. Hence, the transverse motions at $z = 0$ are very efficiently converted into longitudinal motions; this conversion essentially occurs near levels where $\beta = 1$. These calculations support our earlier results using the thin flux tube approximation [69-70], which showed the efficient generation of longitudinal waves due to mode coupling fairly low in the atmosphere. In addition, they allow one to follow the propagation of MHD waves into the chromosphere, where a 1-D treatment breaks down.

4. Summary

The purpose of this review was to discuss various processes associated with intense magnetic fields in the surface layers of the Sun's atmosphere. Magnetic fields emerge in the photosphere from the solar interior as large coherent flux tubes which fragment into regions occurring at the boundaries of supergranule cells called the enhanced network. The emerging flux concentrations have field strengths that are unlikely to exceed the dynamic equipartition value, which is much smaller than the observed value in the network. It is generally believed that this field is further strengthened by a combination of *flux expulsion* and *convective collapse*; the latter is associated with an instability which operates preferentially in the sub-photosphere and produces intense flux tubes with fields in the kilogauss range. Support for this mechanism comes through a prediction of a relationship between the size (radius) and field strength, which shows qualitative agreement with observations.

Flux tubes in the magnetic network are likely to play an important role in heating the chromosphere. Their footpoints, located in the sub-photosphere, are constantly buffeted by granules, due to which MHD oscillations are excited in the tubes. Detailed calculations confirm that the low frequency waves observed in the network can be identified mainly with kink or transverse MHD waves in a thin flux tube with a period that corresponds to the cutoff period for kink waves. In the photospheric layers, most of the energy is in kink waves – however, in the chromosphere longitudinal waves are generated due to nonlinear effects – their characteristic signature is an oscillation at the

longitudinal cutoff period. Longitudinal waves, being compressible, form shocks and thereby contribute to chromospheric heating. The incompressible kink waves, on the other hand, can propagate through the chromosphere and contribute to coronal heating.

Realistic models of the dynamics and heating in the magnetic network need to take into account the expansion and merging of flux tubes in the chromosphere. As a first step, the network field has been modelled as an ensemble of flux tubes, in magnetostatic equilibrium, that are rooted in the photosphere. Transverse motions at the base of the tubes excite fast MHD waves within the tubes and acoustic waves at the interface of the tubes and the field-free medium. The acoustic waves at the interface are due to compression of the gas on one side of the tube and expansion on the other. These oscillations travel upward along the sides of the tube and enter it, where they become longitudinal waves. For impulsive excitation, we find that dominant feature is the creation of vortical motions that propagate upwards. A new and efficient mechanism for the generation of longitudinal waves and shock formation in the chromosphere has been identified.

Acknowledgements: I am grateful to Drs. A. van Ballegooijen, W. Kalkofen, P. Ulmschneider, O. Steiner and K. Sivaraman for helpful discussions.

References

1 Stenflo J O, *Solar Magnetic Fields: Polarized radiation diagnostics*,(Kluwer, Dordrecht), 1994.
2 Solanki S K, *Space Sci. Rev.*, 63 (1993), 1.
3 Thomas J H, Weiss, N O, in *Sunspots: Theory and Observations*, Nato ASI Series C Vol. 375 (Kluwer, Dordrecht), (1992), 3.
4 Bogdan T J, *Sol. Phys.*, 192 (2000), 373.
5 Zwaan C, Harvey K L, in *Solar Magnetic Fields*, eds. M. Schüssler, & W. Schmidt (Cambridge University Press), (1994), 27.
6 Chapman G A, Cookson A M, Dobias J J, *Astrophys. J.*, 482 (1997), 541.
7 Solanki S K, in *Solar and Stellar Activity: Similarities and Differences*, eds. C. J. Butler, & J. G. Doyle, A. S. P. Conf. Series, Vol. 158 (1999), 109.
8 Harvey K L, *Ph. D. Thesis*, Utrecht University, Utrecht (1993).
9 Schrijver C J, Harvey K L, *Sol. Phys.*, 150 (1994), 1.
10 Parker E N, *Astrophys. J*, 138 (1963), 552.
11 Parker E N, *Astrophys. J*, 221 (1978) 368.
12 Weiss N O, *Proc. Roy. Soc.*, A293 (1966), 310.
13 Weiss N O, *J. Fluid Mech.*, 108 (1981), 247.
14 Galloway D J, Proctor M R E, Weiss N O, *J. Fluid Mech.*, 87 (1978), 243.
15 Nordlund Å., in *Solar and Stellar Magnetic Fields: Origins and Coronal Effects* IAU Symp. No. 102, ed. J O Stenflo (Reidel Dordrecht) (1983), 79.
16 Stein R F, Nordlund Å, *Sol. Phys.*, 192, (2000), 91.
17 Webb A R, Roberts B, *Sol. Phys.*, 59 (1978), 249.
18 Spruit H C, Zweibel E G, *Sol. Phys.*, 62 (1979), 15.
19 Unno W, Ando H, *Geophys. Astrophys. Fluid Dyn.* 12 (1979), 107.
20 Rajaguru S P, Hasan S S, *Astrophys. J*, 544 (2000), 522.
21 Hasan S S, in *Solar and Stellar Magnetic Fields: Origins and Coronal Effects* IAU Symp. No. 102, ed. J. O. Stenflo (Reidel, Dordrecht) (1983), 73.
22 Hasan S S, *Astrophys. J*, 285 (1984), 851.
23 Hasan S S, *Astron. Astrophys.*, 143 (1985), 39.
24 Venkatakrishnan P, *J. Astrophys. Astron.*, 4 (1983), 135.

25 Venkatakrishnan P, *J. Astrophys. Astron.*, 6 (1985), 21.
26 Takeuchi A, *Pub. Astron. Soc. Japan*, 45 (1993), 811.
27 Takeuchi A, *Pub. Astron. Soc. Japan*, 47 (1995), 331.
28 Grossmann-Doerth U, Schüssler M, Steiner O, *Astron. Astrophys.*, 337 (1998), 928.
29 Hasan S S, van Ballegooijen A A, in *Cool Stars Stellar Systems and the Sun, Tenth Cambridge Workshop*, eds. R. A. Donahue & J. Bookbinder, A. S. P. Conf. Series, Vol. 154 (1998), 630.
30 Hasan S S, *Mon. Not. R. Astr. Soc.*, 219 (1986), 357.
31 Solanki S K, Zufferey D, Lin H, Rüedi I, Kuhn J R, *Astron. Astrophys.*, 310 (1996), L33.
32 Lin H, *Astrophys. J.*, 446 (1995), 421.
33 Lin H, Rimmele T, *Astrophys. J.*, 514 (1999), 448.
34 Sánchez Almeida J, Lites B W, *Astrophys. J.* 532 (2000), 1215.
35 Skumanich A, Smythe C, Frazier E N, *Astrophys. J.*, 200 (1975), 747.
36 Lites B W, Rutten R J, Kalkofen W, *Astrophys. J.*, 414 (1993), 345.
37 Curdt W, Heinzel P, *Astrophys. J.*, 503 (1998), L95.
38 McAteer R T J, Gallagher P, Williams D, Mathioudakis M, Phillips K J H, Keenan F P, *Astrophys. J.*, 567 (2002), L168.
39 McAteer R T J, Gallagher P T, Williams D R, et al, *Astrophys. J.* 587 (2003), 806.
40 Grossmann-Doerth U, Kneer F, von Uexküll M, *Sol. Phys.* 37 (1974), 85.
41 Carlsson M, Stein R F, *Astrophys. J.* 440 (1995), L29.
42 Roberts B, Ulmschneider P, in *Lecture Notes in Physics* (Springer Verlag, Heidelberg), Vol. 489 (1998), 75.
43 Defouw R J, *Astrophys. J.*, 209 (1976), 266.
44 Roberts B, Webb A R *Sol. Phys.*, 56 (1978), 5.
45 Ryutov D D, Ryutova M P, *Sov. Phys. JETP* 43, (1976), 491.
46 Parker E N, *Cosmical Magnetic Fields: Their origin and their activity* (Clarendon Press, Oxford) (1979).
47 Spruit H C, *Sol. Phys.*, 75 (1982), 3.
48 Lighthill M J, *Proc. Roy. Soc. London*, A211 (1952), 564.
49 Osterbrock D E, *Astrophys. J.*, 134 (1961), 347.
50 Musielak Z E, Rosner R, *Astrophys. J.*, 315 (1987), 371.
51 Collins W, *Astrophys. J.*, 337 (1989), 548.
52 Collins W, *Astrophys. J.*, 384 (1992), 39.
53 Musielak Z E, Rosner R, Ulmschneider P, *Astrophys. J.*, 437 (1989), 470.
54 Musielak Z E, Rosner R, Gail H P, Ulmschneider P, *Astrophys. J.*, 448 (1995), 865.
55 Huang P, Musielak Z E, Ulmschneider P, *Astron. Astrophys.*, 297 (1995), 579.
56 Ulmschneider P, Musielak Z E, *Astron. Astrophys.* 338 (1998), 311.
57 Muller R, Roudier Th, *Sol. Phys.*, 141 (1992), 27.
58 Muller R, Roudier Th, Vigneau J, Auffret H, *Astron. Astrophys.* 283 (1994), 232.
59 Choudhuri A R, Auffret H, Priest E R, *Sol. Phys.* 143 (1993), 49.
60 Choudhuri A R, Dikpati M, Banerjee D, *Astrophys. J.* 413 (1993), 811.
61 Steiner O, Grossmann-Doerth U, Knölker M, Schüssler M, *Astrophys. J.* 495 (1998), 468.
62 Hasan S S, Kalkofen W, *Astrophys. J.* 519 (1999), 899.
63 Kalkofen W, *Astrophys. J.* 486 (1997), L145.
64 Hasan S S, Kalkofen W, van Ballegooijen A A, *Astrophys. J.*, 535 (2000), L67.
65 Ulmschneider P, in *Space Solar Physics, theoretical and observational issues in the context of the SOHO mission* eds. J. C. Vial, K. Bocchialini, & P. Boumier (Springer Verlag, Berlin) (1998), 77.

66 Avrett E H, in *Chromospheric Diagnostics and Modelling* ed. B. Lites (Sunspot, New Mexico) (1985), 67.
67 Ulmschneider P, Zähringer K, Musielak Z E, *Astron. Astrophys.*, 241 (1991), 625.
68 Zhugzhda Y D, Bromm V, Ulmschneider P, *Astron. Astrophys.*, 300 (1995), 302.
69 Hasan S S, Kalkofen W, van Ballegooijen A A, Ulmschneider P, *Astrophys. J.*, 585 (2003), 1138.
70 Hasan S S, Ulmschneider P, *Astron. Astrophys.*, 422 (2004), 1085.
71 Ulmschneider P, Kalkofen W, Nowak T, Bohn H U, *Astron. Astrophys.*, 54 (1977), 61.
72 Ulmschneider P, in Lectures on Solar Physics, eds. H.M. Antia, A. Bhatnagar & P. Ulmschneider, *Lecture Notes in Physics* (Springer Verlag, Heidelberg, Berlin), 619 (2003), 232.
73 Rosenthal C S, Bogdan T J, Carlsson M, Dorch S B F, Hansteen V, McIntosh S W, McMurry A, Nordlund Å, Stein R F, *Astrophys. J.*, 564 (2002), 508.
74 Bogdan T J, Carlsson M, Hansteen V, McMurry A, Rosenthal C S, Johnson M, Petty-Powell S, Zita E J, Stein R F, McIntosh S W, Nordlund Å, *Astrophys. J.*, 599 (2003), 626.
75 Cranmer S R, van Ballegooijen A A, *Astrophys. J. Suppl.*, 156 (2005), 265.
76 Hasan S S, van Ballegooijen A A, Kalkofen W, Steiner O, *Astrophys. J.*, (2005), (in press).